

Non-invasive load measurement in the human tibia via spectral analysis of flexural waves

Ali Yawar*† and Daniel E. Lieberman

Department of Human Evolutionary Biology, Harvard University, Cambridge MA, USA

Abstract

Forces transmitted by bones are routinely studied in human biomechanics, but it is challenging to measure them non-invasively, especially outside of the laboratory setting. We introduce a technique for non-invasive, *in vivo* measurement of tibial compression force using flexural waves propagating in the tibia. Modeling the tibia as an axially compressed Euler-Bernoulli beam, we show that tibial flexural waves have load-dependent frequency spectra. Specifically, under physiological conditions, peak locations in the acceleration amplitude spectrum shift linearly with the compression force on the tibia, and may be used as proxy force measure. We test the validity of this technique using a proof-of-principle wearable system that generates flexural waves via a skin-mounted mechanical transducer and measures the spectra of these waves using a skin-mounted accelerometer. In agreement with beam theory, data from three participants demonstrate linear relationships between tibial compression force and peak frequency location with Pearson correlation coefficients $r = 0.88\text{--}0.97$ for medial-lateral swaying and $r = 0.88\text{--}0.95$ for walking trials. Our flexural wave-based technique could give rise to a new class of wearable sensors for non-invasive physiological load monitoring and measurement, impacting research in human locomotion, sports medicine, and prosthetic design.

1 Introduction

The human tibia is subjected to a dynamic combination of bending, twisting, and axial loading during locomotion. In running, the tibia can sustain compression forces reaching up to 14 times the bodyweight [Scott and Winter, 1990]. A majority of the tibial compression force is attributed to tension from triceps surae muscle contractions during propulsion [Matijevich et al., 2019]. Tibial compressive loading, like loading in other bones, impacts maintenance [Kohrt et al., 2004], growth [Robling and Turner, 2009], and injury [Moen et al., 2009, Warden et al., 2014], and is therefore a key variable to measure in experimental human biomechanics.

Currently, in laboratory or clinical settings, a standard technique to estimate bone loading uses optical motion capture and instrumented treadmills along with inverse dynamics models [Winter, 2009]. A more invasive method relies on strain gauges embedded directly within the bone, with gauge placement limited to the medial diaphysis of the tibia in humans [Milgrom et al., 2004, Rubin, 2001, Yang et al., 2011]. For in-field use, the primary tools are wearable inertial measurement units (IMUs) or insole pressure sensors which measure bone load proxies like tibial acceleration or ground reaction force [Elstub et al., 2022, Willy et al., 2025]. But despite decades of research and use, wearable IMU based proxies are not reliable surrogates for bone loading [Matijevich et al., 2019, Xiang et al., 2024]. Recent machine learning based

*Address correspondence to: aliyawar92@gmail.com.

†Current affiliation: Amazon Robotics, North Reading, MA, USA. The work in this paper was completed prior to this author's affiliation with Amazon.

approaches yield better accuracy, but the inherent subject-specific modeling assumptions and lack of interpretability hamper their broad applicability [Matijevich et al., 2020].

We introduce a non-invasive technique that uses propagating flexural waves in the tibia to measure compressive loading. In a beam-like structure like the tibia, flexural wave propagation is governed by material and geometric properties and the axial load borne by the structure [Doyle, 2020]. Tibial flexural waves have previously been used for non-invasive monitoring of material properties [Fäh and Stüssi, 1988, Stüssi and Fäh, 1988], but their relationship with tibial load has not been studied. Modeling the tibia as an axially compressed Euler-Bernoulli beam, we show that its mechanical impedance is load-dependent, and consequently flexural waves in the tibia have a frequency spectrum that changes with the compression force on the tibia. Thus, the force on the tibia may be inferred by tracking variations in the wave spectra. We demonstrate this technique using a proof-of-principle, non-invasive wearable system in three participants performing medial-lateral swaying (at approx. 0.3 Hz) and walking (0.4 m/s) on an instrumented treadmill, and compare our measurements against ground-truth tibial compression force measured using inverse dynamics. The non-invasive and portable nature of our technique has implications for the development of new wearable sensors for in-field measurements and continuous monitoring of bone loading in athletic, clinical, or industrial environments.

2 Results

2.1 Flexural wave propagation model

We model the tibia as a uniform, infinitely long Euler-Bernoulli beam with density ρ , cross sectional moment of inertia I , Young's modulus E , and cross sectional area A (figure 1A). The beam is loaded with a uniform axial compression force P . The governing equation for transverse displacement $y(x, t)$ is

$$EI \frac{\partial^4 y}{\partial x^4} + P \frac{\partial^2 y}{\partial x^2} + \rho A \frac{\partial^2 y}{\partial t^2} = 0, \quad (1)$$

where x, t are the axial spatial coordinate and time, respectively. We solve equation (1) in the frequency (ω) domain following Doyle [2020]. At $x = 0$, the transducer (figure 1A) applies a transverse force $f(t)$ with Fourier transform $\mathcal{F}(\omega)$. Combining this force boundary condition with the condition for symmetric wave generation at $x = 0$ (see Supplemental Materials for details), we solve equation (1) to get the spectrum of transverse displacement at a location $x \gg 0$,

$$\mathcal{Y}(P, \omega, x) = \frac{-i\mathcal{F}}{2EI(\xi^3 + \xi\kappa^2)} e^{-i\xi x}, \quad (2)$$

where $\xi, \kappa \in \mathbb{R}^+$ are load- and frequency-dependent wavenumbers defined by,

$$\xi(P, \omega) = \frac{\sqrt{P + \sqrt{P + 4\rho IE A \omega^2}}}{\sqrt{2EI}}, \quad \kappa(P, \omega) = \frac{\sqrt{-P + \sqrt{P + 4\rho IE A \omega^2}}}{\sqrt{2EI}}. \quad (3)$$

The transfer impedance of the beam between the origin and a fixed measurement location $x = x_m$ is defined as

$$\mathcal{Z}(P, \omega) = \frac{\mathcal{F}}{\omega \mathcal{Y}(P, \omega, x_m)}, \quad (4)$$

and its magnitude is found using equation (2) as

$$Z_P(\omega) \equiv |\mathcal{Z}(P, \omega)| = \frac{2EI(\xi^3 + \xi\kappa^2)}{\omega}. \quad (5)$$

The normalized impedance magnitude Z_P/Z_0 is plotted against frequency ω in figure 1B, assuming $\mathcal{F}(\omega)$ is identical at all loads. For $P > 0$, the impedance shows two distinct regimes, separated by a load-dependent cutoff frequency $\omega_c = P/2\sqrt{\rho IE A}$. For frequencies $\omega \gg \omega_c$,

axial compression has no effect on impedance as $Z_P/Z_0 \approx 1$. At lower frequencies ($\omega \ll \omega_c$), as $Z_P/Z_0 > 1$, the compressed beam has a higher impedance than the beam with zero load.

A measurable effect of the beam's load-dependent impedance is that the acceleration (or velocity or displacement) spectrum of flexural waves will shift towards higher frequencies with increasing compression force. Consequently, if the magnitude of the acceleration spectrum for the zero-load beam has a peak at ω^* , impedance change due to a small axial load ($0 < P \ll EA$) will cause a shift in the spectral peak location given by

$$\Delta\omega^* = \frac{P}{4\sqrt{\rho I E A}} \frac{\gamma(\omega^*)}{\omega^{*2}}, \quad (6)$$

where $\gamma(\omega^*)$ is a parameter that depends on the sharpness of the spectral peak at zero-load (equation (S22)). Thus, the spectral peak location shifts linearly with the compression force on the tibia. Assuming constant material and geometric properties of the tibia, equation (6) may be used to infer relative changes in the tibial compression force by measuring shifts in the locations of peaks in the flexural wave acceleration spectra in the tibia.

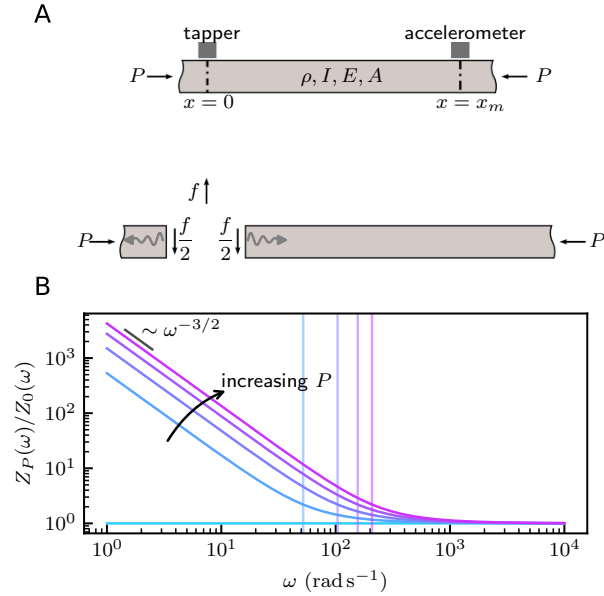


Figure 1. Axially compressed Euler-Bernoulli beam model. **A** Beam with density ρ , cross-sectional moment of inertia I , Young's modulus E , and cross-sectional area A , supports a uniform axial load P , which is positive in compression. A transducer at $x = 0$ applies a transverse force $f(t)$ to the beam. As a result, a flexural disturbance propagates symmetrically away from the origin (shown by wavy arrows) which is measured by an accelerometer located at $x_m \gg 0$. **B** Log-log plot of the transverse impedance magnitude normalized by the zero-load impedance $Z_P(\omega)/Z_0(\omega)$ versus frequency ω . Colors denote a range of axial compression loads ($0 \leq P \leq 5000$ N). The normalized impedance shows two distinct regimes separated by a load-dependent cutoff frequency $\omega_c = P/2\sqrt{\rho I E A}$ (marked by vertical lines). Under nonzero loads, $Z_P > Z_0$ for $\omega \ll \omega_c$, and $Z_P \approx Z_0$ for $\omega \gg \omega_c$. Parameter values for this plot are based on published values for the human tibia: $\rho = 1850$ kg m⁻³, $E = 20$ GPa, $I = 10^{-8}$ m⁴, $A = 2.5 \times 10^{-4}$ m² [Minns et al., 1975, Rho, 1996].

2.2 Implementation of the sensor system

The above derivation considers the beam's flexural response to a force input $f(t)$. If the duration of $f(t)$ and the resulting response of the tibia are short enough (akin to a "tap"), the tibial

compression force may be assumed constant over the duration of the tap, and the flexural wave spectrum may be considered stationary. If a periodic sequence of identical taps is applied to the tibia, the flexural wave generated in response to each tap will correspond to the tibial compression force at the instant of the tap, assuming that successive waves can be temporally separated. In this way by measuring the response of successive flexural waves, tibial loading may be continually tracked at a sampling rate equal to the rate of tapping. In our setup, a skin-mounted audio transducer (or “tapper”) near the medial malleolus delivers a sequence of impulsive taps at 50 Hz to generate a train of flexural waves in the tibia. These waves are monitored using a skin-mounted accelerometer near the proximal end of the tibia (figure 2A,B). The flexural wave acceleration response to a single tap shows that the wave settles well before the subsequent tap is initiated (figure 2C). Peaks in the spectrum of the flexural wave acceleration are then identified and used to infer the compression force on the tibia (figure 2D).

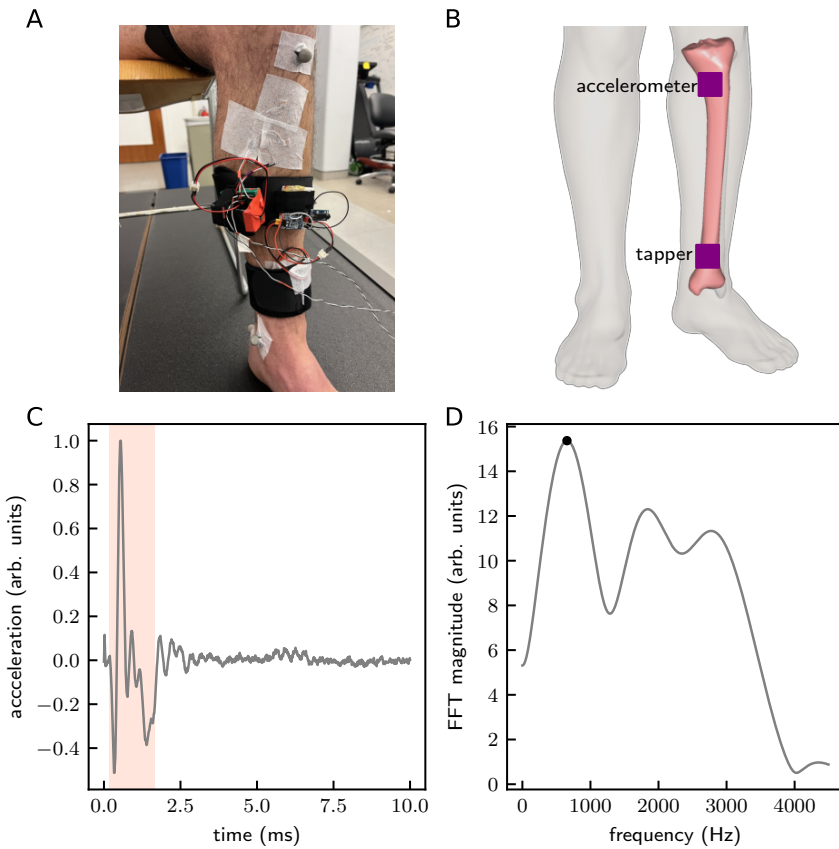


Figure 2. Overview of the sensor setup and measurements. **A**, Photograph of a participant’s left leg showing the system setup and **B**, approximate locations of the audio transducer (“tapper”) and accelerometer on a schematic of the tibia. **C** The measured transverse acceleration in response to a single tap initiated at $t = 0$ s. The signal is sampled at 100 kHz, mean-centered and normalized by the maximum acceleration. The portion of the acceleration signal used in analyses is highlighted in pink. **D** Frequency domain representation of the highlighted acceleration signal shown in panel C, via the amplitude of the Fast Fourier Transform (FFT). Subsequent analyses use the location of the amplitude spectrum peak (solid black dot) to infer the compression force on the tibia. The leg and tibia schematics are from BodyParts3D [Mitsuhashi et al., 2009], used under a CC-BY-SA license.

2.3 In vivo measurement of flexural wave spectra

Using our wearable system, we perform measurements of flexural wave spectra in the left tibia of participants as they perform a medial-lateral swaying trial on an instrumented treadmill, during which the tibia undergoes an approximately periodic compressive loading (~ 3 Hz). The time-varying spectra of acceleration from one participant are shown in figure 3A as a spectrogram spanning the duration of the trial (30 s). Each vertical slice of figure 3A shows the amplitude of the acceleration spectrum in response to a single tap. The spectrogram has a ridge of peaks fluctuating around ~ 600 Hz (black curve). The extracted peaks correspond strongly with the ground-truth tibial compression force measurement over the duration of the trial (figure 3B), with a Pearson correlation coefficient, $r = 0.94$ (figure 3C). The correlation coefficients for the other two participants for medial-lateral swaying trials are $r = 0.97, 0.88$ respectively (figures S1,S3).

We also measure the flexural wave spectrum in participants walking at 0.4 m/s. Figure 4A shows data from one participant, comprising the ensemble mean and standard deviation of the extracted spectral peaks (red) and the ground-truth tibial compression force (blue), both normalized to the duration of stance. Over the entire trial, the spectral peaks were correlated with ground-truth tibial compression force with a Pearson correlation coefficient, $r = 0.95$ (figure 4B). The correlation coefficients for the other two participants for walking trials are $r = 0.94, 0.88$ respectively (figures S2,S4).

3 Discussion

We have demonstrated that flexural waves may be used to measure the *in vivo* compression force on the tibia. Our model of the tibia as an axially compressed Euler-Bernoulli beam shows that the impedance of the tibia is load-dependent. Because of this load-dependent impedance, assuming identical flexural wave sources, the flexural wave spectrum shifts towards higher frequencies under higher compression force. Consequently, any peaks in the flexural wave spectrum will shift to higher frequencies with increasing tibial compression force. Using a skin-mounted audio transducer at the distal end of the tibia, we generate a train of propagating flexural waves from which spectral peaks are identified using a skin-mounted accelerometer at the proximal end of the tibia. In agreement with predictions of the beam model, we see a strong linear relationship between compression force on the tibia and spectral peak locations in the flexural wave acceleration spectrum (figures 3,4). While in our implementation the participant is tethered to signal generators and data acquisition equipment, all of the requisite processing may be accomplished by lightweight hardware worn on the body. To prevent a tripping hazard and tugging of the electronics by the tethering cables, our experiments involved only medial-lateral swaying and slow walking trials (0.4 m/s). But since the peak frequencies tracked in our experiments are above 600 Hz, we expect the measurements to be robust to disturbance from vibration even in high-impact running, where the noise is typically around 30 Hz or lower [Chadefaux et al., 2019, Horvais et al., 2019]. This robustness against additive noise is also evidenced in our methods, as the acceleration data required no filtering. Thus, our technique is well-suited for incorporation into a low-cost, portable, wearable sensor system similar to recently developed wearable shear-wave tensiometers for tendon load measurement [Martin et al., 2018, Reiter et al., 2024].

While it is not the primary topic of this study, we note that the phase of the flexural wave acceleration spectrum is also load-dependent (equation (2)). At a specific frequency and at a fixed measurement location, the phase increases linearly with the compression force on the tibia (equation (S23)). However, in our implementation, the phase measurements required trial-specific filtering of the acceleration data and showed poorer linear correlations with load for most trials, making phase a less suitable target as compared to the spectral amplitude. The poor signal to noise ratio (SNR) is possibly because phase measurement using the FFT is highly sensitive to the range of the signal captured within the FFT aperture, which varies with load given the dispersive nature of flexural waves and the load-dependence of the wave spectrum.

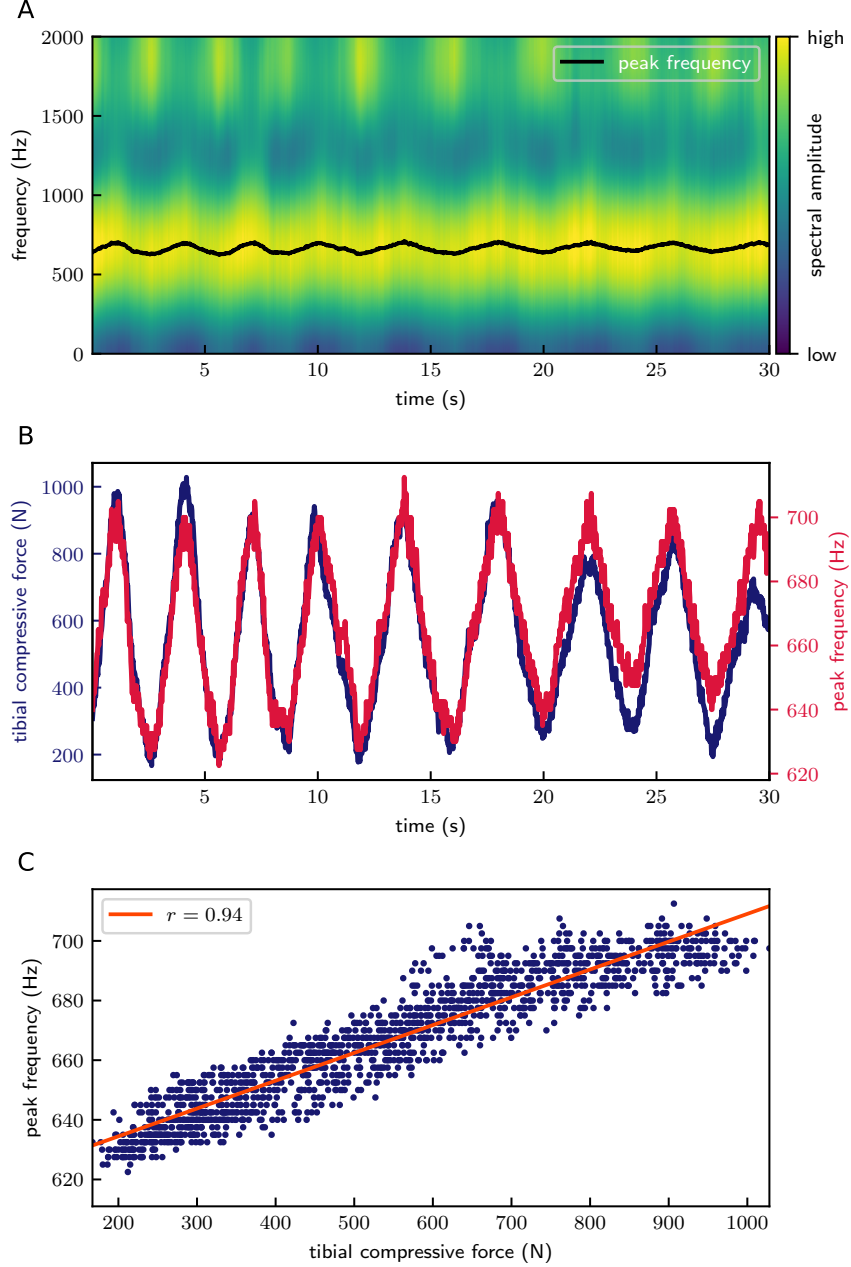


Figure 3. Tibial compression force measurement in a medial-lateral swaying trial. **A**, Spectrogram of the flexural wave accelerations measured in response to a periodic sequence of taps delivered at 50 Hz. Each vertical line is the spectrum of the acceleration response of a single tap, and the amplitude of the spectrum, in arbitrary units, is denoted by color. Peak frequencies in the spectrum are marked by the black curve. **B**, Overlaid on the peak frequency measure (red), the force measured using motion capture and inverse dynamics (blue) shows strong correspondence over the trial duration. **C**, Scatter plot of the two measures over the entire trial, showing a linear dependence with a Pearson correlation coefficient, $r = 0.94$. The linear regression line is shown in red. Data from the other two participants is reported in supplementary figures S1, S3.

As the ground-truth measurement of tibial compression force, we use the sum of ankle joint force along the tibia, and Achilles tendon tension, following Matijevich et al. [2019]. Achilles

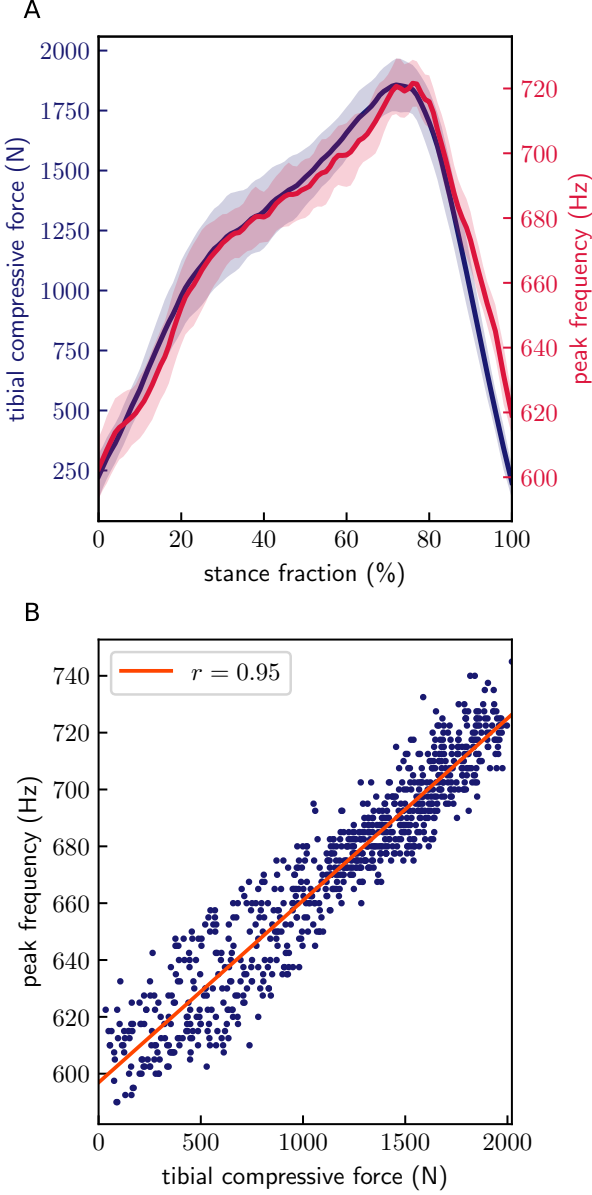


Figure 4. Tibial compression force measurement in a walking trial. **A**, Ensemble averaged data from the walking trial of one participant, showing the correspondence between ground-truth tibial force (blue curve) and the peak frequency measurement (red curve). Data are averaged over 17 steps, and normalized over the period of stance with heel strike at 0% and toe off at 100%. Solid curves show the means, and shaded region spans one standard deviation above and below the mean. **B** Scatter plot of the two measures for the entire trial from the same participant, showing a linear dependence with a Pearson correlation coefficient, $r = 0.95$. The linear regression line is shown in red. Data from the other two participants is reported in supplementary figures S2, S4.

tension is defined as ankle sagittal moment divided by a constant Achilles tendon moment arm [Matijevich et al., 2019]. This simplification ignores contributions of the other large muscles spanning the tibia like the tibialis posterior/anterior, and the toe flexors and extensors, all of which contribute to the compression of the tibia during dynamic movements. More complex muscle models in future studies may help identify more precise limits of flexural wave-based

measurements.

Our choices of system parameters such as the locations of the tapper and accelerometer, tapper force profile, sampling rate, etc. were selected to accomplish a simple proof-of-principle implementation of the flexural wave-based load measurement technique. Future implementations may benefit from empirical studies to determine the parameter combinations for the most optimal SNR, taking into account the expected noise characteristics in each specific use case.

There are a few limitations to our technique. First, our accelerometer measurements are not feasible on body locations that have significant subcutaneous fat, muscles, or tendons. These soft tissues can dampen skin-mounted acceleration measurements compared to more precise bone-mounted measurements on the tibia [Nokes et al., 1984]. Muscle contraction can additionally generate confounding acceleration signals. While preloading the accelerometers may reduce the amount of damping by skin and other soft tissues [Nokes et al., 1984], the associated signal distortion may render the measurement unusable, especially if consistent preload can not be maintained. Second, the spectrum of flexural waves in our model only depends on the *net* compression force on the tibia and cannot resolve stress gradients across the tibial cross-section, which may arise due to bending or torsion of the tibia during load bearing [Wallace et al., 2014, Yang et al., 2014]. Thus, our method here only measures one aspect of how the tibia is loaded. Finally, separation between successive taps needs to be enough to allow the response of the tibia from one tap to be quiescent before the next tap is delivered. Thus, there is a fundamental upper limit on the rate at which tibial compression forces can be measured with this technique.

Spectral analysis of flexural waves in bone may serve as a simple and low cost target for commercial wearable sensor development in the future.

Such sensors would enable in-field measurement and monitoring of tibial loading, allowing experimental studies with sample sizes and study durations that are currently infeasible. For example, prospective studies on large samples of athletic populations may be performed in natural settings to help answer persistent questions on the causes and prevention of repetitive stress injuries. The almost real-time measurements allowed by this technique may enable continuous monitoring of tibial loading. Such monitoring may be helpful in ensuring better movement form in athletes and manual material handlers by providing live feedback during physical activity. Continuous monitoring of tibial compression forces may also enable better tuning of prosthetic compliance and fit for orthopedic rehabilitation.

4 Methods and materials

4.1 Participants

We recruited $N = 3$ participants (1 male, 2 females; age 27.3 ± 1.7 years, body mass 78.8 ± 16.4 kg, mean \pm s.d.) with no recent history of lower limb injury. The study protocol was approved by the Committee on the Use of Human Subjects at Harvard University. Each participant provided written informed consent.

4.2 Data collection

Kinematic and kinetic data

Retro-reflective markers were placed on 9 bony landmarks: greater trochanter, medial and lateral epicondyles of the femur, tibial tuberosity, medial and lateral malleoli, posterior calcaneus inferior to the insertion location of the Achilles tendon, and heads of the 1st and 5th metatarsals. Kinematic data were collected using an eight camera motion capture system (Qualisys AB, Gothenburg, Sweden) at 200 Hz. Force data were collected using an instrumented treadmill (Bertec, Columbus, OH, USA) at 2000 Hz. Both force and kinematic data were filtered using a 2nd order Butterworth lowpass filter at a 25 Hz cutoff frequency. Data were initially processed in Visual3D (C-Motion, Inc., Moys, MD, USA) and subsequently in Python v3.11.5. For the medial-lateral swaying task, the treadmill belt was stopped and participants were asked to stand

in a neutral posture and then slowly shift their weight from one foot to another without lifting either foot from the treadmill. Participants swayed at approximately 3 Hz. The walking trials were performed at 0.4 m/s. The slow walking speed ensured that the tethering cables were not a tripping hazard and did not tug on the sensitive electronics worn by the participants.

As the ground-truth measurement, compression force on the tibia was estimated as the sum of two forces: i) the ankle joint force projected onto the long axis of the tibia, and ii) the sagittal plane ankle moment divided by the moment arm of the Achilles tendon, assumed constant for each participant (5 cm) [Matijevich et al., 2019]. Time instants when the vertical ground reaction force was below 20 N or when the center of pressure was posterior to the ankle were excluded from the analyses.

Accelerometer

Flexural wave acceleration was measured using a piezoelectric voice accelerometer (VA1200, Vesper Inc., MA, USA). The SMD accelerometer was soldered to a small, flexible printed circuit board (6.4 mm by 6.6 mm “Flex” style PCB, OSH Park LLC, OR, USA). Terminals on the circuit board were soldered to 31 gauge wires, and subsequently connected to shielded coaxial cables, from which the accelerometer voltage was sampled at 100 kHz. The thin, flexible wires attached to the PCB were meant to reduce the inertial effects of the coaxial cables on the accelerometer. The PCB was placed near the proximal end of the tibia such that the accelerometer was directly in contact with the skin. The PCB was secured using athletic gauze tape (BSN Cover-Roll Stretch, Hamburg, Germany). The accelerometer was powered using a 3V Alkaline battery pack. The voltage output from the accelerometer was AC coupled and amplified using PowerLab ML880 (ADIInstruments).

Audio transducer

We used a 1 W “bone conduction” audio transducer (Product # 1674, Adafruit Inc., NY, USA) to deliver periodic force perturbations (“taps”). This transducer was actuated using a square wave (10 V, 50 Hz) generated by LabChart v8.1.30 (ADIInstruments) and amplified using a 2.5 W audio amplifier (PAM8302, Adafruit Inc., NY, USA). A 3.7 V LiPo battery was used as power supply for the amplifier. Shielded coaxial cables were used to transmit the square wave signal to the amplifier to minimize interference. The tapping device was secured directly to skin at the distal end of the tibia using athletic gauze tape, and then further secured using velcro fabric bands typically used with wearable IMUs. Flexural waves were generated by taps from both the rising and falling edges of the square wave, but only the rising edge taps were considered for analysis in this study. The separation between the transducer and accelerometer was about 20 cm.

Spectral analysis

A 1.5 ms length of the unfiltered acceleration signal, starting at 0.15 ms after each tap, was used for analysis. Each window was mean centered and normalized by the maximum acceleration within the window. This data was windowed using a cosine window of the same length. The windowed signal was converted to its frequency spectrum using the Fast Fourier Transform algorithm with 40000 bins. The large FFT size led to efficient sinc interpolation of the spectrum and allowed better resolution for peak identification. Finally, isolated peaks were identified in the amplitude spectrum and tracked using a generic peak finding algorithm. When necessary, the range of the peak finding algorithm was restricted to prevent jumping among peaks in the spectrum.

Statistical analyses

Pearson correlation coefficients were calculated between the ground-truth tibial compression forces and the measured spectral peak locations over the entirety of each trial. Walking data were ensemble averaged over all complete recorded steps. A 20 N vertical ground reaction force threshold was used to identify foot contact events, and the data were normalized to lie between 0% (heel strike) and 100% (toe off) of stance.

Acknowledgements

We thank V. Joshi, K. Nguyen, A. Ravan, E. Reimink, and N. Sharma for helpful discussions and feedback at various stages of this study. A.Y. acknowledges support from the American School of Prehistoric Research (Harvard University).

Author contributions

AY conceived of the study, and designed the study in consultation with DEL. AY performed mathematical modeling, built the experimental apparatus, and collected and analyzed data. AY wrote the paper with inputs from DEL.

References

D. Chadefaux, N. Gueguen, A. Thouze, and G. Rao. 3d propagation of the shock-induced vibrations through the whole lower-limb during running. *Journal of Biomechanics*, 96:109343, 2019.

J. F. Doyle. *Wave Propagation in Structures*. Springer Cham, 2020.

L. Elstub, C. Nurse, L. Grohowski, P. Volgyesi, D. Wolf, and K. Zelik. Tibial bone forces can be monitored using shoe-worn wearable sensors during running. *Journal of sports sciences*, 40(15):1741–1749, 2022.

D. Fäh and E. Stüssi. Phase velocity measurement of flexural waves in human tibia. *Journal of biomechanics*, 21(11):975–983, 1988.

K. F. Graff. *Wave motion in elastic solids*. Dover Publications, 1991.

N. Horvais, P. Samozino, X. Chiementin, J.-B. Morin, and M. Giandolini. Cushioning perception is associated with both tibia acceleration peak and vibration magnitude in heel-toe running. *Footwear Science*, 11(1):35–44, 2019.

W. M. Kohrt, S. A. Bloomfield, K. D. Little, M. E. Nelson, and V. R. Yingling. Physical activity and bone health. *Medicine & Science in Sports & Exercise*, 36(11):1985–1996, 2004.

J. A. Martin, S. C. Brandon, E. M. Keuler, J. R. Hermus, A. C. Ehlers, D. J. Segalman, M. S. Allen, and D. G. Thelen. Gauging force by tapping tendons. *Nature communications*, 9(1):1592, 2018.

E. S. Matijevich, L. M. Branscombe, L. R. Scott, and K. E. Zelik. Ground reaction force metrics are not strongly correlated with tibial bone load when running across speeds and slopes: Implications for science, sport and wearable tech. *PloS one*, 14(1):e0210000, 2019.

E. S. Matijevich, L. R. Scott, P. Volgyesi, K. H. Derry, and K. E. Zelik. Combining wearable sensor signals, machine learning and biomechanics to estimate tibial bone force and damage during running. *Human movement science*, 74:102690, 2020.

C. Milgrom, A. Finestone, A. Hamel, V. Mandes, D. Burr, and N. Sharkey. A comparison of bone strain measurements at anatomically relevant sites using surface gauges versus strain gauged bone staples. *Journal of biomechanics*, 37(6):947–952, 2004.

R. Minns, G. Bremble, and J. Campbell. The geometrical properties of the human tibia. *Journal of Biomechanics*, 8(3-4):253–255, 1975.

N. Mitsuhashi, K. Fujieda, T. Tamura, S. Kawamoto, T. Takagi, and K. Okubo. Bodyparts3d: 3d structure database for anatomical concepts. *Nucleic acids research*, 37(suppl_1):D782–D785, 2009.

M. H. Moen, J. L. Tol, A. Weir, M. Steunebrink, and T. C. De Winter. Medial tibial stress syndrome: a critical review. *Sports medicine*, 39:523–546, 2009.

L. Nokes, J. Fairclough, W. Mintowt-Czyz, I. Mackie, and J. Williams. Vibration analysis of human tibia: the effect of soft tissue on the output from skin-mounted accelerometers. *Journal of biomedical engineering*, 6(3):223–226, 1984.

A. J. Reiter, J. A. Martin, K. A. Knurr, P. G. Adamczyk, and D. G. Thelen. Achilles tendon loading during running estimated via shear wave tensiometry: a step towards wearable kinetic analysis. *Medicine and science in sports and exercise*, 56(6):1077, 2024.

J.-Y. Rho. An ultrasonic method for measuring the elastic properties of human tibial cortical and cancellous bone. *Ultrasonics*, 34(8):777–783, 1996.

A. G. Robling and C. H. Turner. Mechanical signaling for bone modeling and remodeling. *Critical Reviews™ in Eukaryotic Gene Expression*, 19(4), 2009.

C. T. Rubin. In vivo measurement of bone deformations using strain gauges. *Bone mechanics handbook*, 2001.

S. H. Scott and D. A. Winter. Internal forces at chronic running injury sites. *Medicine & Science in Sports & Exercise*, 22(3):357–369, 1990.

E. Stüssi and D. Fäh. Assessment of bone mineral content by in vivo measurement of flexural wave velocities. *Medical and Biological Engineering and Computing*, 26(4):349–354, 1988.

I. J. Wallace, B. Demes, C. Mongle, O. M. Pearson, J. D. Polk, and D. E. Lieberman. Exercise-induced bone formation is poorly linked to local strain magnitude in the sheep tibia. *PLoS one*, 9(6):e99108, 2014.

S. J. Warden, I. S. Davis, and M. Fredericson. Management and prevention of bone stress injuries in long-distance runners. *Journal of orthopaedic & sports physical therapy*, 44(10):749–765, 2014.

R. W. Willy, K. Christensen, B. Hanser, M. Plemmons, and B. C. Ruby. Average vertical loading rate and tibial accelerometry are not valid assessments of internal tibial loads when walking or running with or without load carriage: A cross-sectional laboratory study. *Journal of Sports Sciences*, 0(0):1–11, 2025.

D. A. Winter. *Biomechanics and motor control of human movement*. John Wiley & Sons, 2009.

L. Xiang, Z. Gao, A. Wang, V. Shim, G. Fekete, Y. Gu, and J. Fernandez. Rethinking running biomechanics: a critical review of ground reaction forces, tibial bone loading, and the role of wearable sensors. *Frontiers in Bioengineering and Biotechnology*, 12:1377383, 2024.

P. Yang, G.-P. Brüggemann, and J. Rittweger. What do we currently know from in vivo bone strain measurements in humans? *Journal of Musculoskeletal and Neuronal Interactions*, 11(1):8–20, 2011.

P.-F. Yang, M. Sanno, B. Ganse, T. Koy, G.-P. Brüggemann, L. P. Müller, and J. Rittweger. Torsion and antero-posterior bending in the in vivo human tibia loading regimes during walking and running. *PLoS one*, 9(4):e94525, 2014.

5 Supplemental material

5.1 General far-field solution for propagating flexural waves

In this section, we derive expressions for the spectra of propagating flexural waves in the axially compressed tibia, following Doyle [2020] and Graff [1991]. We model the tibia as an infinitely long Euler-Bernoulli beam with uniform density ρ , cross-sectional moment of inertia I , Young's modulus E , and cross-sectional area A . A uniform compression force P is applied along the long axis of the tibia. The governing partial differential equation is

$$EI \frac{\partial^4 y}{\partial x^4} + P \frac{\partial^2 y}{\partial x^2} + \rho A \frac{\partial^2 y}{\partial t^2} = 0, \quad (\text{S1})$$

where x is the axial coordinate, t is time, $y(x, t)$ is the transverse displacement. With the radius of gyration $r = \sqrt{E/A}$ as the length scale, the speed of sound in the medium $c = \sqrt{E/\rho}$ to define the time scale r/c , and axial rigidity EA as the force scale, we non-dimensionalize the variables in equation (S1) using the following definitions

$$\hat{x} \equiv \frac{x}{r}, \quad \hat{t} \equiv \frac{tc}{r}, \quad \hat{P} \equiv \frac{P}{EA}. \quad (\text{S2})$$

The dimensionless Euler-Bernoulli equation is given by

$$\frac{\partial^4 \hat{y}}{\partial \hat{x}^4} + \hat{P} \frac{\partial^2 \hat{y}}{\partial \hat{x}^2} + \frac{\partial^2 \hat{y}}{\partial \hat{t}^2} = 0, \quad (\text{S3})$$

We solve equation (S3) in the frequency-domain to obtain a solution of the form $\mathcal{Y}(\hat{x}, \hat{\omega})$ that specifies the frequency spectrum of the beam's transverse displacement at a location \hat{x} on the beam. This spectrum is defined via the Fourier transform as $\hat{y}(\hat{x}, \hat{\omega}) = \int_{-\infty}^{\infty} \hat{y}(\hat{x}, \hat{t}) e^{-i\hat{\omega}\hat{t}} d\hat{t}$. Applying the Fourier transform to equation (S3) we get the spectral form of the Euler-Bernoulli equation,

$$\frac{d^4 \hat{\mathcal{Y}}}{d\hat{x}^4} + \hat{P} \frac{d^2 \hat{\mathcal{Y}}}{d\hat{x}^2} - \hat{\omega}^2 \hat{\mathcal{Y}} = 0. \quad (\text{S4})$$

The general solution to this ordinary differential equation is given by $\mathcal{Y} = Y(\hat{k}) e^{i\hat{k}\hat{x}}$, where $\hat{k} \equiv \hat{k}(\hat{\omega}) \in \mathbb{C}$, is a frequency-dependent wavenumber satisfying the characteristic equation

$$\hat{k}^4 + \hat{P}\hat{k}^2 - \hat{\omega}^2 = 0. \quad (\text{S5})$$

There are two real and two imaginary solutions for the wavenumber given by $\hat{k} = \pm i\hat{\xi}, \pm \hat{\kappa}$ where

$$\hat{\xi}(\hat{P}, \hat{\omega}) = \sqrt{\frac{\hat{P} + \sqrt{\hat{P}^2 + 4\hat{\omega}^2}}{2}}, \quad \hat{\kappa}(\hat{P}, \hat{\omega}) = \sqrt{\frac{-\hat{P} + \sqrt{\hat{P}^2 + 4\hat{\omega}^2}}{2}}, \quad (\text{S6})$$

and $\hat{\xi}, \hat{\kappa} \in \mathbb{R}^+$. Rewriting these in dimensionful form yields the expression in equation (3) in the main text.

We can then write the general solution in the frequency domain as $\hat{\mathcal{Y}} = C_1 e^{-i\hat{\xi}\hat{x}} + C_2 e^{-\hat{\kappa}\hat{x}} + C_3 e^{i\hat{\xi}\hat{x}} + C_4 e^{\hat{\kappa}\hat{x}}$, where C_n are complex-valued functions of $\hat{\omega}$. The general solution consists of a forward (along positive \hat{x}) and a backward traveling wave. We restrict our focus to the forward traveling solutions given by

$$\hat{\mathcal{Y}} = C_1 e^{-i\hat{\xi}\hat{x}} + C_2 e^{-\hat{\kappa}\hat{x}} \quad (\text{S7})$$

5.2 Boundary conditions

We require two boundary conditions to solve for the coefficients C_1, C_2 . For the first boundary condition, we assume that the resulting waves travel symmetrically outward from the point of tapping ($\hat{x} = 0$) giving us the boundary condition $d\hat{y}/d\hat{x} = 0$. Applying this boundary condition to equation (S7) we get $C_2 = -i(\hat{\xi}/\hat{\kappa})C_1$, so that the solution can be written with a single unknown coefficient as,

$$\hat{\mathcal{Y}} = C_1 (e^{-i\hat{\xi}\hat{x}} - i \frac{\hat{\xi}}{\hat{\kappa}} e^{-\hat{\kappa}\hat{x}}). \quad (\text{S8})$$

We solve for C_1 using the force balance equation at the location of tapping, $\hat{x} = 0$. Assume a force $\hat{f}(\hat{t})$ is applied to a massless particle of the beam located at $\hat{x} = 0$. The force balance at that point is

$\hat{f} + 2\hat{v} = m\hat{y} = 0$, where $\hat{v} = -\partial^3\hat{y}/\partial\hat{x}^3$ is the shear force associated with the deformation of the beam. If the Fourier transform of the applied force $\hat{f}(\hat{t})$ is $\hat{\mathcal{F}}(\hat{\omega})$, we get

$$\hat{\mathcal{F}} - 2 \frac{d^3\hat{\mathcal{Y}}}{d\hat{x}^3} \Big|_{\hat{x}=0} = 0 \implies C_1 = \frac{-i\hat{\mathcal{F}}}{2(\hat{\xi}^3 + \hat{\xi}\hat{\kappa}^2)}. \quad (\text{S9})$$

From equations (S8) and (S9), the complete frequency domain solution for the transverse flexural wave acceleration is given by

$$\hat{\mathcal{A}} = -\hat{\omega}^2\hat{\mathcal{Y}} = \frac{i\hat{\omega}^2\hat{\mathcal{F}}}{2(\hat{\xi}^3 + \hat{\xi}\hat{\kappa}^2)}(e^{-i\hat{\xi}\hat{x}} - i\frac{\hat{\xi}}{\hat{\kappa}}e^{-i\hat{\kappa}\hat{x}}). \quad (\text{S10})$$

Note that the acceleration spectrum is a function of $\hat{\omega}$, \hat{P} and \hat{x} . Far from the load application point ($\hat{x} \gg 0$), the spatially (“near-field”) term vanishes, and the solution is simplified to the far-field limit

$$\hat{\mathcal{A}} = \frac{i\hat{\omega}^2\hat{\mathcal{F}}}{2(\hat{\xi}^3 + \hat{\xi}\hat{\kappa}^2)}e^{-i\hat{\xi}\hat{x}}. \quad (\text{S11})$$

5.3 Load-dependence of peaks in the acceleration magnitude spectrum

To derive the dependence of the acceleration spectrum on the tibial compression force, we introduce the transfer impedance of the beam, which is defined as the ratio of the force at the origin, and velocity at \hat{x}_m ,

$$\hat{\mathcal{Z}} \equiv \frac{\hat{\mathcal{F}}}{\hat{\omega}\hat{\mathcal{Y}}} = \frac{\hat{\omega}\hat{\mathcal{F}}}{\hat{\mathcal{A}}}. \quad (\text{S12})$$

Using the impedance here allows us to derive a general relationship between flexural wave spectra and axial load. As seen in figure 1, as axial load increases, the impedance selectively suppresses lower frequencies. One measurable consequence of this phenomenon is that any peaks in the acceleration spectrum would shift to higher frequencies under higher loads. We rewrite equation (S12) as

$$\hat{\mathcal{A}}(\hat{P}) = \frac{\hat{\omega}\hat{\mathcal{F}}}{\hat{\mathcal{Z}}(\hat{P}, \hat{\omega})}. \quad (\text{S13})$$

Defining the magnitude (or amplitude) of the acceleration spectrum $\hat{a} \equiv |\hat{\mathcal{A}}|$ and normalizing by the zero load acceleration spectrum we can write

$$\frac{\hat{a}(\hat{P}, \hat{\omega})}{\hat{a}_0(\hat{\omega})} = \frac{\hat{\mathcal{Z}}(0, \hat{\omega})}{\hat{\mathcal{Z}}(\hat{P}, \hat{\omega})} \equiv M(\hat{P}, \hat{\omega}), \quad (\text{S14})$$

where $\hat{a}_0(\hat{\omega}) \equiv \hat{a}(0, \hat{\omega})$. At $\hat{P} = 0$, we assume that the acceleration spectrum has a peak $\hat{\omega}^*$, so that $a'_0(\hat{\omega}^*) = 0$, where prime denotes derivative with respect to $\hat{\omega}$.

We note that for the human tibia, Young’s modulus $E \approx 20$ GPa, and cross sectional area at the tibial mid-shaft $A \approx 2.5 \times 10^{-4}$ m², resulting in a flexural rigidity of about 5×10^6 N. So, under physiological loads the dimensionless compression force on the tibia $\hat{P} \approx 10^{-4} \ll 1$. At a small compression force $0 < \hat{P} \ll 1$, let the peak of the acceleration magnitude shift to a nearby frequency $\hat{\omega}^* + \Delta\hat{\omega}$, so that $a'(\hat{P}, \hat{\omega}^* + \Delta\hat{\omega}) = 0$. Differentiating $\hat{a}(\hat{P}, \hat{\omega})$ with respect to $\hat{\omega}$ in equation (S14) we get

$$\hat{a}'(\hat{P}, \hat{\omega}) = M'(\hat{P}, \hat{\omega})\hat{a}_0 + M(\hat{P}, \hat{\omega})\hat{a}'_0. \quad (\text{S15})$$

To evaluate equation (S15) at a small load \hat{P} and at a frequency $\hat{\omega}^* + \Delta\hat{\omega}$, we use linear approximations of \hat{a}_0, \hat{a}'_0 around $\hat{\omega} = \hat{\omega}^*$, and of M, M' around $\hat{P} = 0$ and $\hat{\omega} = \hat{\omega}^*$:

$$\hat{a}_0(\hat{\omega}^* + \Delta\hat{\omega}) \approx \hat{a}_0(\hat{\omega}^*) \quad (\text{S16})$$

$$\hat{a}'_0(\hat{\omega}^* + \Delta\hat{\omega}) \approx \hat{a}''_0(\hat{\omega}^*)\Delta\hat{\omega} \quad (\text{S17})$$

$$M(\hat{P}, \hat{\omega}^* + \Delta\hat{\omega}) \approx M(0, \hat{\omega}^*) + \hat{P} \frac{\partial M}{\partial \hat{P}} \Big|_{0, \hat{\omega}^*} + \Delta\hat{\omega} \frac{\partial M}{\partial \hat{\omega}} \Big|_{0, \hat{\omega}^*} = 1 - \frac{\hat{P}}{4\hat{\omega}^*} \quad (\text{S18})$$

$$M'(\hat{P}, \hat{\omega}^* + \Delta\hat{\omega}) \approx M'(0, \hat{\omega}^*) + \hat{P} \frac{\partial M'}{\partial \hat{P}} \Big|_{0, \hat{\omega}^*} + \Delta\hat{\omega} \frac{\partial M'}{\partial \hat{\omega}} \Big|_{0, \hat{\omega}^*} = \frac{\hat{P}}{4\hat{\omega}^{*2}}. \quad (\text{S19})$$

Using equations (S16) — (S19) to evaluate equation (S15), we can finally write,

$$a'(\hat{P}, \hat{\omega}^* + \Delta\hat{\omega}) = \hat{a}_0(\hat{\omega}^*) \frac{\hat{P}}{4\hat{\omega}^{*2}} + \hat{a}_0''(\hat{\omega}^*) \Delta\hat{\omega} \left(1 - \frac{\hat{P}}{4\hat{\omega}^*}\right) = 0 \quad (\text{S20})$$

The change in peak frequency caused by a small increase in the compression force is then given by

$$\Delta\hat{\omega} = -\frac{\hat{a}_0(\hat{\omega}^*)}{\hat{a}_0''(\hat{\omega}^*)} \frac{\hat{P}}{4\hat{\omega}^{*2}}. \quad (\text{S21})$$

Rewritten in dimensionful variables and noting that at a peak, $a_0''(\omega^*) < 0$

$$\Delta\omega = \frac{a_0(\omega^*)}{|a_0''(\omega^*)|} \frac{P}{4\sqrt{\rho I E A} \omega^{*2}}. \quad (\text{S22})$$

This expression yields several insights. First, the higher the peak frequency ω^* at zero load, the smaller the change in peak frequency. This is because at higher frequencies, the impedance of the axially compressed beam approaches that of the zero-load beam. Second, the ratio $a_0/|a_0''|$ in equation (S21) quantifies the sharpness of the spectral peak at zero load. This ratio is governed only by the tapping force $\mathcal{F}(\omega)$, and is independent of the beam's material properties. The sharper the zero load peak, the smaller the ratio and thus smaller the change in peak frequency. In the limit of a zero-load peak that approaches a delta-function, changes in the impedance would only scale the height of the peak and not shift the peak. As long as the resulting spectral peaks can be measured experimentally, equation (S21) can be used to estimate the compression force on the bone.

5.4 Load-dependence of the acceleration phase spectrum

From equation (S11), we see that the phase spectrum of the acceleration also depends on the tibial compression force. The phase is defined as $\phi(\omega) \equiv \arg \hat{\mathcal{A}} = -\hat{\xi} \hat{x}_m$. Normalizing the phase at a small compression force $\hat{P} \ll 1$ by the zero-load phase and linearizing around $\hat{P} = 0$ we get,

$$\frac{\phi}{\phi_0} = (1 + \frac{\hat{P}}{4\hat{\omega}}) \hat{x}_m \equiv 1 + \frac{P}{4\omega \sqrt{\rho I E A}}. \quad (\text{S23})$$

Thus, at any frequency, the phase difference measured for a propagating flexural wave has an affine dependence on the compression force P .

5.5 Supplemental data figures

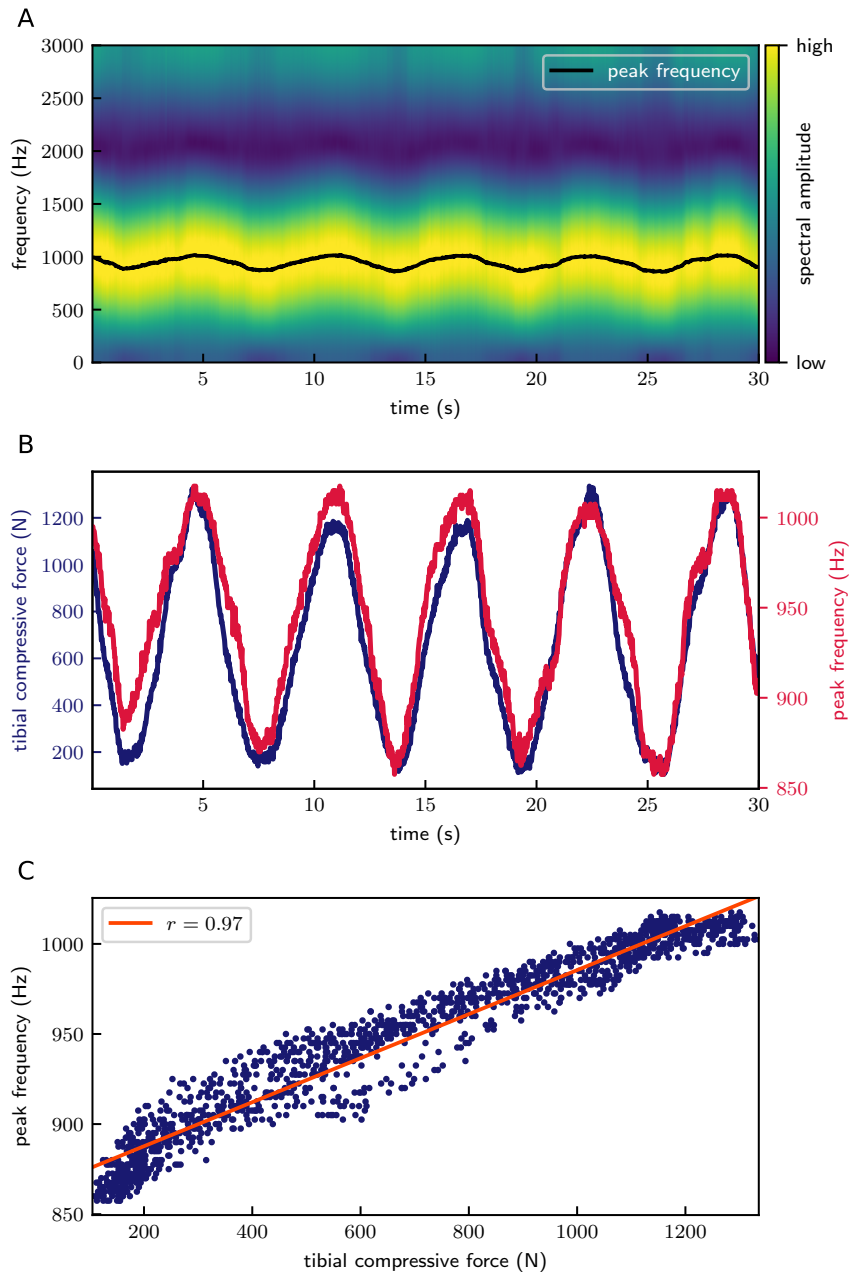


Figure S1. Data from medial-lateral swaying trial of participant 2.

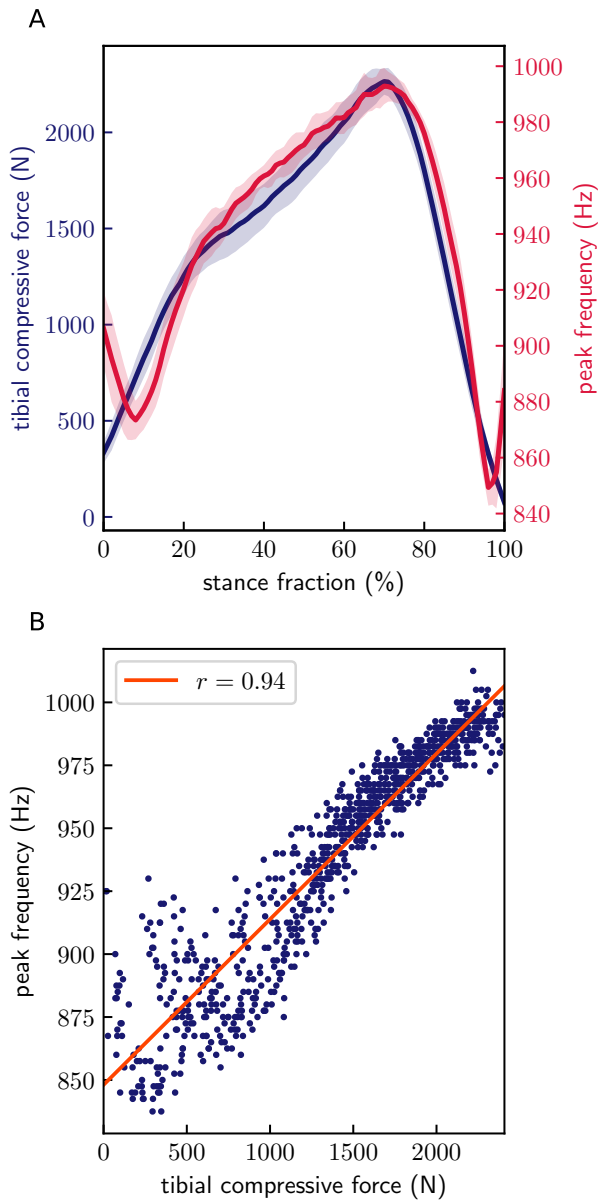


Figure S2. Data from walking trial of participant 2. Data in panel A are ensemble-averaged over 16 steps.

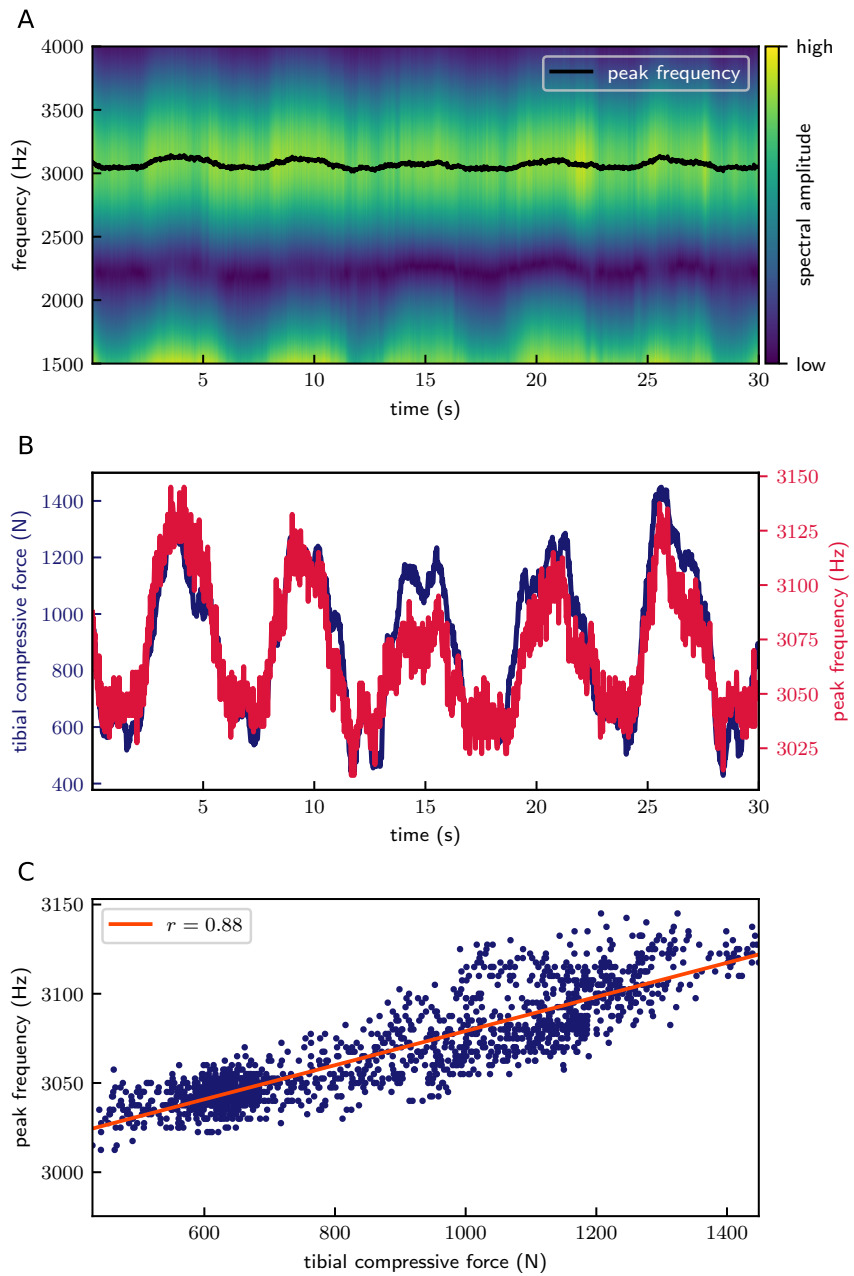


Figure S3. Data from medial-lateral swaying trial of participant 3.

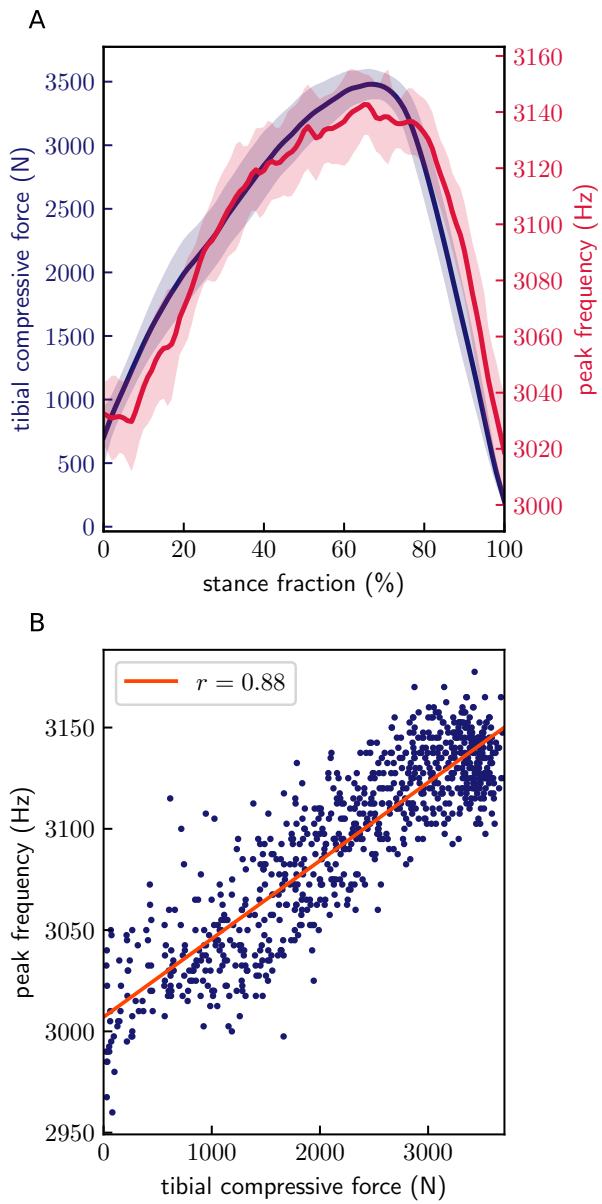


Figure S4. Data from walking trial of participant 3. Data in panel A are ensemble-averaged over 19 steps.